Lipid multilayered particles: the role of chitosan on structure and morphology†

Yuri Gerelli,*[a] Maria Teresa Di Bari,[a] Antonio Deriu,[a] Daniel Clemens[b] and László Almásy[cd]

Received 24th November 2009, Accepted 11th March 2010
First published as an Advance Article on the web 29th April 2010
DOI: 10.1039/b924616a

Multilayered nanovectors made up from a controlled binary lipid mixture (POPC and DMPS) and trimethyl chitosan (TMC) have been prepared and characterized by light- and small angle neutron scattering. The morphology and the multilayer structure of the particle outer shell has been described in detail. By varying the amount of TMC in the starting solution it is possible to tune the overall surface particle charge as well as its multilamellarity. In this way the drug loading/release properties of the particles can be controlled. Therefore the use of controlled POPC/DMPS mixtures can be a valid alternative to commercial lecithin to obtain nanovectors with specific release properties.

1 Introduction

Nowadays nanotechnologies are having an increasing impact in various fields of medicine, providing significant innovation in therapy, diagnostics, imaging and drug delivery.[1,2] Since the mid '90s colloidal carriers have been used for the administration of drugs with biopharmaceutical problems, such as severe side effects, low stability in biological fluids, specific organ toxicity, low bioavailability and, above all, poor aqueous solubility. Encapsulation into nanosized carriers modifies the interaction of the drug molecules with the biological environment. It is then possible to protect the drug from chemical and enzymatic degradation and to tune the kinetics of the release process. Moreover, localization of the active species in specific cell types within target organs can be obtained by addition of targeting ligands to the particle surface.[3,4] Nanoparticles suitable as drug delivery systems can be built up using a variety of materials including polymers (polymeric nanoparticles, micelles, or dendrimers),[4] lipids (liposomes),[5] gels and hydrogels,[6] microemulsions[7] and viruses (viral nanoparticles).[8] Lipid based nanovectors are self-assembled colloidal particles with an outer lipid bilayer or multilayer shell, surrounding a central aqueous core (liposomes). Among these systems, great attention has been given to particles obtained from ionic lipids with polyelectrolytes as "stabilizing" agents.[9–11] In fact, in pure liposomal systems, the interaction between the carrier and the surrounding environment cannot be accurately controlled; as a consequence the release process cannot be tuned in time and space. To overcome these limitations, surface modifications have been tested: in particular lipid-DNA[12,13] and lipid-saccharide complexes[14–17] have been investigated in detail. The first ones have been developed as an alternative to viral vehicles for delivering genes into mammalian cells, while lipid-saccharide complexes are more effective in improving the solubility of lipophilic drugs and in extending the life-time of the circulating vector.[18,19] In a previous study we investigated the complexation mechanism between a mixture of anionic lipids (commercial lecithin: Lipoid S45) and a positively charged polysaccharide (chitosan) and the effect of the latter on the structure of the nanoparticles.[20] The nanoparticles were characterized by an aqueous hollow core surrounded by a multilayer structure made up of lipid bilayers and interlayer regions containing water and chitosan. The lecithin/chitosan ratio strongly affected the multilamellarity of the outer shell. The high number of components (different lipids and fatty acids) present in commercial lecithin and the polydispersity of the resulting nanoparticles made it difficult to analyze the internal features of the lipid multilayers in detail. We have now replaced commercial lecithin with a well defined binary mixture of highly purified lipids: 98% 1-palmitoyl-2-oleoyl-sn-*glycero*-3-phosphocholine (POPC) and 2% 1,2-dimyristoyl-sn-glycero-3-[phospho-L-serine] (DMPS). We have also replaced the polyion component with trimethyl chitosan (TMC) whose positive charge is pH independent.[21,22] The structure and morphology of the obtained nanoparticles have been investigated by dynamic light scattering (DLS), ζ-potential measurements and small angle neutron scattering (SANS).

2 Experimental

In order to get detailed structural information on multicomponent nanoparticles commercial lecithin has been replaced by a controlled binary lipid mixture (98% POPC and 2% DMPS from Avanti Polar Lipids Inc., Alabama (US)); partially deuterated POPC (indicated in the following as POPC(d31)) has also been adopted. Their chemical structures are reported in Fig. 1. POPC is a common lipid with an unsaturated bond in the oleic tail; DMPS has a shorter tail with one negative charge in the headgroup for each molecule. Using 98/2 POPC/DMPS mixture, we have obtained self-assembled liposomes with surface charge and size similar to that of lecithin vesicles investigated by us in

[a]*Dipartimento di Fisica, Università degli Studi di Parma, CNISM, INFM-CNR, Parma, Italy. E-mail: Yuri.Gerelli@fis.unipr.it*
[b]*Helmholtz-Zentrum Berlin für Materialien und Energie, Berlin, Germany*
[c]*Laboratory for Neutron Scattering, PSI and ETH Zürich, CH-5232 Villigen, Switzerland*
[d]*Adolphe Merkle Institute, University of Fribourg, CH-1700 Fribourg, Switzerland*

† Electronic supplementary information (ESI) available: POPC and POPC/DMPS liposomes, and form factor for the SANS analysis. See DOI: 10.1039/b924616a

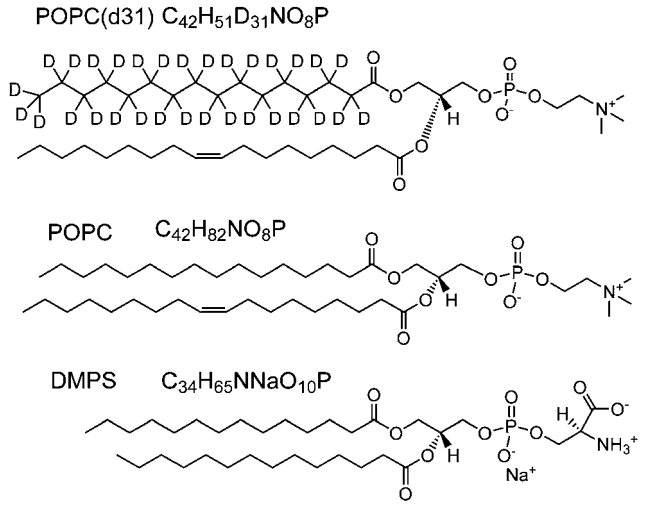

Fig. 1 The chemical structures of partially deuterated POPC, POPC and DMPS molecules used for the sample preparation.

a previous work.[20] Chitosan is a polysaccharide obtained from N-deacetylation of chitin. It is normally insoluble in aqueous solution above pH 7; nevertheless, in dilute acids, the free amino groups are protonated and the molecule becomes fully soluble below ~pH 5.[23] To overcome this pH dependence of the solubility we have used trimethyl chitosan (TMC) (from Medipol SA, Switzerland) obtained by addition of a methyl group to each amine side-chain group (see Fig. 2). Its nominal molecular weight is ~105 kDa with a substitution degree of ~60%.

POPC/DMPS/TMC nanoparticles (indicated in the following as NCM) were prepared from different starting solutions: (i) 200 mg of POPC/DMPS dissolved in 8 ml of ethanol, (ii) three solutions of TMC in 92 ml of water (D_2O, H_2O or H_2O/D_2O) previously filtered through 200 μm polycarbonate membranes, and different TMC amounts in order to obtain the following final TMC/lipids ratios: 1 : 12, 1 : 7, 1 : 4 (w/w). The NCM particles were obtained by rapid injection (nozzle diameter 0.75 mm, injection rate 40 ml min^{-1}), under mechanical stirring, of the ethanol solution into the TMC aqueous one. The self-assembling process gave rise to a colloidal suspension with pH 7 and nanoparticle concentration $c = 0.2\%$ by weight. The particles are indicated in the following as NCM12, NCM7 and NCM4. The NCM7 suspension is very close to the isoelectric point of the solution, the others have a higher TMC content and therefore bring an overall positive charge. It is worth noticing that the lipid/saccharide ratios adopted here differ from those previously used for the preparation of lecithin-based nanoparticles:[14,20] this is due to the different degree of quaternization and molecular weight of TMC with respect to chitosan. With the adopted composition, the present NCM particles are equivalent, in terms of their surface charge and hydrodynamic radius, to the ones investigated previously. In order to obtain detailed information on the spatial arrangement of the different components, we have used, for the SANS measurements, the contrast variation method. Samples with partially deuterated lipids have been prepared in a 100% D_2O buffer, samples with hydrogenous lipids have been prepared in both 100% D_2O and in a 12/10 D_2O/H_2O mixture that has matched the coherent scattering signal arising from the hydrated lipid headgroups. For comparison purposes three further samples have been analyzed: pure lecithin vesicles (Lipoid in the text), pure POPC/DMPS vesicles in absence of TMC and NCM7 with a concentration $c = 1\%$.

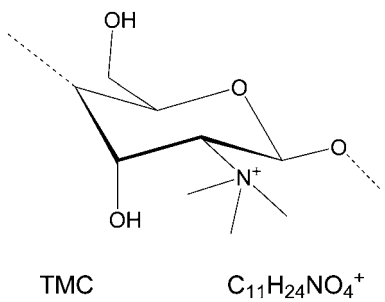

Fig. 2 The chemical structure of a trimethyl chitosan monomer.

2.1 Dynamic laser light scattering

The particle size distribution has been determined (in the range 20–50000 Å) by DLS (90plus, Brookhaven Instruments Corporation, US), using a solid state red laser ($\lambda = 658$ nm) and a $2\theta = 90°$ scattering geometry. The surface charge of the nanoparticles has been obtained by ζ-potential measurements using a phase analysis light scattering apparatus (ZetaPals, Brookhaven Instruments Corporation, US).

2.2 Small angle neutron scattering

SANS experiments have been performed at the BER-II reactor of the Helmholtz-Zentrum-Berlin (Germany) and at the Swiss Spallation Neutron Source (SINQ, Paul Scherrer Institut, CH) using the V4 and the SANS-II diffractometers respectively. Using three different instrument configurations (wavelength λ and sample-to-detector distance D) on both diffractometers we have covered a Q-range of about two decades from 3×10^{-3} to 0.4 $Å^{-1}$ on V4 and from 5×10^{-3} to 0.2 $Å^{-1}$ on SANS-II. The adopted configurations were:

- V4: $\lambda = 6$ Å, $D = 1$ m; $\lambda = 6$ Å, $D = 4$ m; $\lambda = 10$ Å, $D = 16$ m.
- SANS-II: $\lambda = 5.31$ Å, $D = 1.5$ m; $\lambda = 5.31$ Å, $D = 6$ m; $\lambda = 10.6$ Å, $D = 6$ m.

The sample holders were standard quartz flat cells, 1 mm thick for samples prepared in H_2O/D_2O buffers, 2 mm thick for samples measured in D_2O. In this way a similar transmission of about 80% was obtained for all the samples. Standard corrections, cell subtraction and normalization to absolute scattering units have been performed using the BerSANS software.[24]

3 Data analysis

3.1 DLS

The field correlation function $g_2(t)$ has been analyzed in terms of two stretched exponential decays:

$$g_2(t) = A_1 e^{-(t/\tau_1)\beta_1} + (1 - A_1) e^{-(t/\tau_2)\beta_2} + bkg \quad (1)$$

where bkg is a background level; decay times τ_1, τ_2 and stretching parameters β_1, β_2 are related to single particles (index 1) and

particle aggregates (index 2) respectively; A_1 is the intensity weighted fraction of isolated particles. The *n-th* order momentum of the τ distribution is:[25]

$$\langle \tau^n \rangle = \frac{\tau^n}{\beta} \Gamma\left(\frac{n}{\beta}\right) \quad (2)$$

The polydispersity index σ is defined as the ratio $s/\langle\tau\rangle$ between the standard deviation s and the average value $\langle\tau\rangle$. The average hydrodynamic particle radius, $\langle R_{h1}\rangle$, is then obtained applying the well known Stokes–Einstein relation:

$$\langle R_{h1} \rangle = \frac{k_B T Q^2}{6\pi\eta} \langle \tau_1 \rangle \quad (3)$$

where k_B is the Boltzman's constant, T is the temperature, η is the solvent viscosity and $Q = \frac{4\pi n_0}{\lambda}\sin(\theta)$ is the scattering vector (in our case $Q = 1.8 \times 10^{-3}\text{Å}^{-1}$); n_0 is the refractive index of the sample. The hydrodynamic radius of particle aggregates can be derived in the same way. Typical fits obtained by eqn (1) are shown in Fig. 3 for POPC/DMPS liposomes and NCM7 particles.

3.2 SANS

In order to compare the hydrodynamic radii derived from DLS with the radii of gyration, R_g, the SANS data have been analyzed in the low-Q region ($Q_{max}R_g \leq 1$), using the Guinier approximation:

$$I(Q) \propto \exp\frac{-R_g^2 Q^2}{3} \quad (4)$$

On the other hand, to investigate the internal particle structure, the data have been fitted, in the whole Q-range available, using an analytical model describing the scattering intensity.

For multi-lamellar vesicles a detailed picture of the lipid bilayer is provided by the three-strip model.[26–28] For polydisperse particles we have adopted a Schultz distribution $D(\sigma_R, \langle R_0\rangle)$ with average core radius $\langle R_0\rangle$ and polydispersity index σ_R.[29] The differential scattering cross section becomes then:

$$\frac{d\Sigma(Q)}{d\Omega} = \phi \int_0^{+\infty} dr\, D(\sigma_R, \langle R_0\rangle)|F(Q,r)|^2 \quad (5)$$

where ϕ is the particle number density. In order to take into account the presence of particles with different number of layers in the multi-lamellar structure a further Schultz distribution $D(\sigma_N, \langle N\rangle)$, with centroid $\langle N\rangle$ and polydispersity index σ_N, has been introduced:

$$\frac{d\Sigma(Q)}{d\Omega} = \int_0^{+\infty} dN\, D(\sigma_N, \langle N\rangle) \int_0^{+\infty} dr\, D(\sigma_R, \langle R_0\rangle)|F(Q,r,N)|^2 \quad (6)$$

where $F(Q, r, N)$ is the form factor for a particle with N homocentric bilayers. It accounts for the spatial arrangement of the particle components that can be highlighted or hidden upon isotopic substitution (for a detailed description see the ESI†). The data have been analyzed in terms of eqn (6) including the instrumental resolution. The use of a well defined POPC/DMPS mixture allowed us to reduce the number of free parameters in eqn (6). They are: σ_N, $\langle N\rangle$, σ_R, $\langle R_0\rangle$, those related to the radial profile of the structure described by the form factor (the polar head-group thickness t_h and the number n_W of hydration water molecules per headgroup) and the distance d between two subsequent bilayers. The variation of the scattering length density across the bilayer, as well as the thickness of the lipid tails, t_t, and the area per lipid molecule A have been calculated for each sample composition and kept fixed in the fit procedure.[30] Model parameters, constraints and free parameters are listed in Table 1. The samples have been measured in three different lipid-solvent configurations (hydrogenous lipids in D_2O, partially deuterated lipids in D_2O and hydrogenous lipids in a 12/10 D_2O/H_2O buffer), and the structure of the vesicles has been assumed to be the same for the three solvent compositions. The resulting datasets have been simultaneously fitted to eqn (6). For each particular contrast, the fit is more sensitive to a specific part of the vesicle. Therefore, the simultaneous fit of several datasets with the same set of structural parameters has improved the accuracy of the analysis.[26,31]

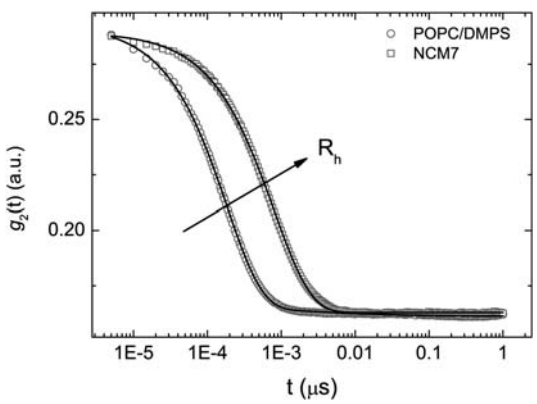

Fig. 3 Field correlation function obtained by DLS for a typical suspension of POPC/DMPS particles (○) and of NCM7 ones (□). The fits according to eqn (1) are shown (—). The change in the shape of the curves with increasing hydrodynamic radius R_h is highlighted by the arrow.

4 Results and discussion

The average size of NCM particles has been determined from DLS, using eqn (1), and from SANS in the Guinier approximation (eqn (4)). DLS gives information related to the Brownian

Table 1 Number of parameters and constraints in the SANS model given by eqn (6). P represents the number of parameters used to model the nanoparticle; in column C the physical constraints are indicated; F = P–C is the number of free parameters in the fit procedure

	P	C	F
Core	2	R_g, σ	2
N. of layers	2		
Head	3	ρ_h^{dry}	2
Tails	2	ρ_t,A	0
Interlayer	3	ρ_{cw}, 2(tt + th)	1
Totals	12	7	5

dynamics of the particles taking into account the existence of a particle hydration shell. It is known that the hydrodynamic radius is usually greater than the real one;[32] the presence of a hydrophilic polyelectrolyte, as chitosan, may enhance this effect. On the other hand, SANS is sensitive to the differences in scattering length densities between the nanoparticle and the surrounding medium: therefore solvent molecules bound to the particle cannot be easily detected by this technique, and the gyration radius provided by SANS is closer to that of the "bare" particle.

In Table 2 the average hydrodynamic radii $\langle R_{h1} \rangle$ derived from DLS and the gyration radii R_g obtained from the SANS data are compared. They coincide, within the experimental error when no TMC is present, while they differ by a factor of ~2 when TMC is added to the preparation. This indicates that in the latter case a thick shell of water molecules closely associated to the particle surface is present. This is not surprising since the presence of positively charged chitosan increases the hydrophilic character of the particle surface. In the case of the NCM12 sample, the low-Q SANS region and the photon field correlation function (DLS) are dominated by the signal of large particle-clusters. In fact the composition of NCM12 particles, in terms of charge balance, is very close to the isoelectric point of the suspension at which phase separation and aggregation occur. For this sample the Guinier analysis of SANS data, and that of DLS data in terms of $g_2(t)$ have not been performed. A further increase of the TMC content above the isoelectric point enhances the absorption of the polyelectrolyte and leads to a positive value of the surface charge as shown in Fig. 4. In going from pure anionic lipids to NCM12, NCM7 and NCM4 the charge of the system is reverted; this fact, together with the crossing of the phase separation region, is indicated as "reentrant condensation" effect.[33–37] It is known that the adsorption of polyelectrolytes on the surface of oppositely charged particles is not only electrostatically driven but it occurs in a highly correlated manner. This correlation, corresponding to a local order of the adsorbed species, results in a short range attraction which can lead to condensation of the polyelectrolytes despite the fact that the surface is already neutralized by the previously adsorbed macroions.

The inner structural features of the NCM particles have been investigated by SANS. The data have been analyzed in terms of eqn (6) in the whole Q-range available: typical fits, for pure lipid samples, are shown in Fig. 5. As expected, pure lipid samples are composed by uni-lamellar POPC/DMPS vesicles with an overall polydispersity index, mainly due to the core-radius distribution, $\sigma = 0.3 \pm 0.1$, in agreement with the value found by DLS ($\sigma = 0.36 \pm 0.09$). Indeed a preliminary fit with free parameters gave: $\langle N \rangle = 1.1 \pm 0.2$ and $\sigma_N = 0 \pm 0.1$; in the subsequent analysis $\langle N \rangle$ and σ_N were then kept fixed to 1 and 0 respectively. The parameters characterizing the lipid bilayer are then $t_h = 9.2 \pm 0.1$ Å, $t_t = 14.9 \pm 0.3$ Å and $A = 62 \pm 3$ Å^2; the number of bound water molecules per polar head group is $n_w = 7 \pm 1$. These values agree with literature data on pure POPC vesicles.[38,39] The presence of 2% of DMPS does not affect the inner structure of the POPC bilayers, while it strongly changes the overall vesicle morphology: in fact a suspension of pure POPC vesicles shows a high presence of multi-lamellar particles. Addition of a small amount of anionic lipids, as 2% of DMPS, favors the formation of uni-lamellar vesicles instead of multi-lamellar ones; this effect is evident in small angle X-ray scattering data (see Fig. S1 in the ESI†). Addition of TMC reverts this effect giving rise to structures similar to those observed in lecithin/chitosan and lipid/DNA complexes: they are characterized by a multi-lamellar arrangement with the polyelectrolyte component (TMC in our case) sandwiched between the lipid bilayers.[13,20] The number of multilayers, $\langle N \rangle$ strongly depends on the lipid/polyion ratio as shown in Fig. 6. On the other hand, addition of TMC does not change appreciably the inner bilayer structure with respect to that of pure lipid vesicles (see Table 3).

The average nanoparticle radii $\langle R \rangle = \langle R_0 \rangle + d \times \langle N \rangle$ are 150 Å for lipid vesicles, 250 Å for NCM7 and 260 Å for NCM4. They

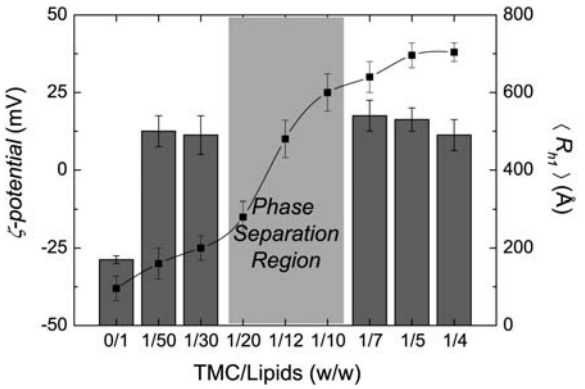

Fig. 4 Average hydrodynamic radius $\langle R_{h1} \rangle$ (bars) and surface charge (■) for NCM at different TMC contents. The phase separation region in which aggregation occurs is marked in gray.

Table 2 Hydrodynamic, $\langle R_{h1} \rangle$, and gyration, R_g, radii obtained from DLS and SANS data. The NCM12 sample was excluded from this analysis due to the presence of large size aggregates

	$\langle R_{h1} \rangle$/Å	R_g/Å
Lipoid	190 ± 10	210 ± 10
POPC/DMPS	170 ± 10	180 ± 5
NCM7	540 ± 50	260 ± 10
NCM4	490 ± 40	240 ± 9

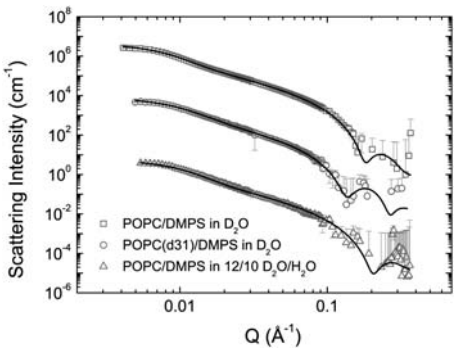

Fig. 5 Scattering profiles of pure lipid vesicles using three different contrast configurations. The change in shape and position of the minimum in the form factor is clearly visible. The intensities have been rescaled to improve the visibility of the curves.

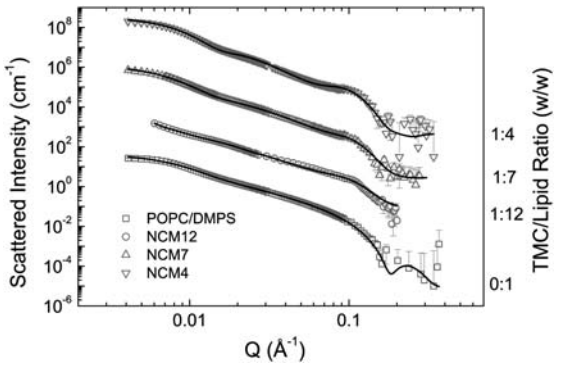

Fig. 6 Scattering profiles for nanoparticles in D_2O at different chitosan/lipid ratio: 1 : 4, 1 : 7, 1 : 12 and pure lipid vesicles (top to bottom). Addition of TMC promotes the formation of an increasing number of multi-lamellar structures detectable by the growth of the correlation peak centered at $Q \sim 0.1$ Å^{-1}. The intensities have been re-scaled to improve the visibility of the curves.

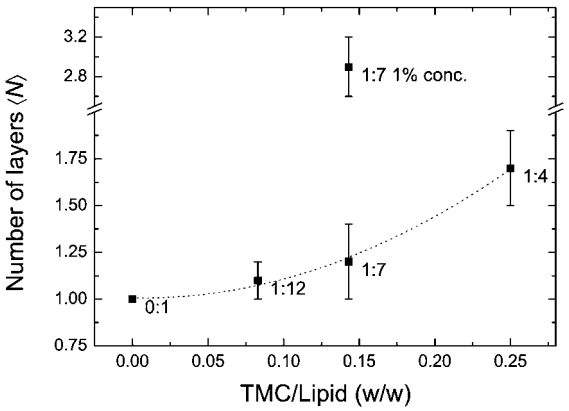

Fig. 7 Average number of bilayers as a function of chitosan content in the starting preparation. The data on NCM7 prepared at higher concentration (1%) are also shown. The dashed curve is drawn as a guide to the eyes.

agree with the ones obtained from the radii of gyration, R_g, within the Guinier-approximation $\left(\langle R\rangle = \sqrt{5/3}\,R_g\right)$. As shown in Fig. 7, in NCM particles a clear correlation exists between the average number of bilayers,$\langle N\rangle$, and the TMC content; such a behavior has not been observed in lecithin-based nanoparticles.[20]

As explained previously, the preparation protocol leads to a suspension with concentration $c = 0.2\%$ w/w. In order to check if the particle structure depends on sample concentration, starting from the NCM7 composition, we have increased by five times the amount of both lipids and saccharides obtaining a suspension with concentration $c = 1\%$. For this sample the DLS analysis shows an average size about three times larger than that of NCM7. The SANS data (intensity and width of the structural peak at $Q \approx 0.12$ Å^{-1}) indicate that this rise is due to an increase of the average number of bilayers surrounding the core (see Fig. 7). Indeed the fit to eqn (6) gives $\langle N\rangle = 3.0 \pm 0.3$ with a polydispersity index $\sigma_N = 0.4 \pm 0.2$ (see Fig. 8). Unfortunately, because of the size of the particles and of the instrumental configuration adopted, it has not been possible to observe the Guinier region and to derive the values of $\langle R_0\rangle$ and σ_R for this sample. Since the hydrodynamic size of NCM7 ($c = 1\%$) has found to be three times larger than that of the same particles at a lower concentration, we expect to observe

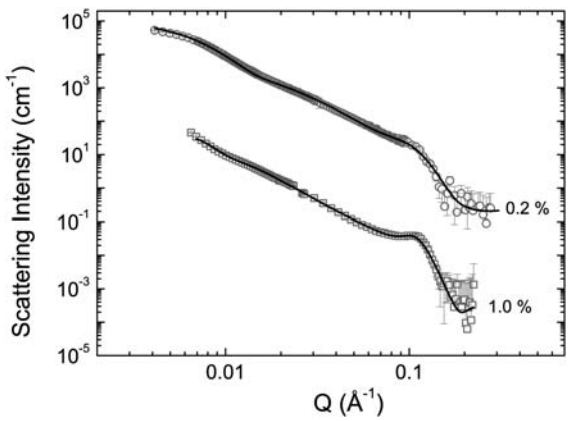

Fig. 8 Scattering profiles for NCM7 in D_2O at the two concentrations investigated: 0.2% (top) and 1% (bottom). The differences in the Q-range are due to the use of different instruments. The intensities have been re-scaled to improve the visibility of the curves.

the Guinier region ($Q_{max}R_g < 1$, with $Q_{max} = 2 \times 10^{-3}$Å^{-1}) in a Q-range not accessible to the instrument used. Concerning the particle inner structure, the parameters characterizing the lipid bilayer are almost unchanged with respect to NCM7 at low concentration.

Table 3 Parameters obtained from the fit of the SANS data to eqn (6). In pure lipid vesicles the inter-layer distance, d, does not appear since they are uni-lamellar. For NCM12 the size of the inner core radius cannot be obtained since the low-Q region of the SANS curves is dominated by the signal due to large particle aggregates

	POPC/DMPS	NCM12	NCM7	NCM4
t_h (Å)	9.2 ± 0.1	9.1 ± 0.3	9.0 ± 0.3	8.8 ± 0.2
t_t (Å)	14.9 ± 0.4	14.5 ± 0.5	13.9 ± 0.5	14.4 ± 0.3
d (Å)	—	62 ± 2	61 ± 1	62.5 ± 0.5
n_w	7 ± 1	8 ± 1	9 ± 1	8 ± 1
A (Å^2)	62 ± 3	63 ± 2	66 ± 2	64 ± 3
$\langle N\rangle$	1 (*fixed*)	1.1 ± 0.1	1.2 ± 0.2	1.7 ± 0.2
$\langle R_0\rangle$ (Å)	100 ± 20	—	180 ± 20	150 ± 10
σ_N	0 (*fixed*)	0.4 ± 0.2	0.33 ± 0.01	0.4 ± 0.1
σ_R	0.2 ± 0.1	—	0.25 ± 0.05	0.3 ± 0.2

5 Conclusions

The combined use of DLS, ζ-potential measurements and SANS gives a clear picture of the structure and morphology of the investigated nanovectors. The presence of TMC does not affect the local structure of the lipid bilayers. On the other hand it is possible to tune the surface charge of the particles in a simple way varying the amount of the charged saccharide component (TMC); this leads to a reentrant condensation effect when the isoelectric point of the suspension is crossed. The amount of TMC, for a given DMPS/POPC ratio in the particles, is a key factor in determining the multilayer structure; in going from a purely anionic solution (zero TMC content) to a 1 : 4 TMC/lipid ratio, the average number $\langle N \rangle$ of bilayers increases continuously from 1 to ~2. A further way to modulate the multilamellarity requires changing the bulk/solvent ratio in the starting solution; this approach has been used for NCM7 particles. The multilayer structure in turn affects the release kinetics of the drugs; therefore the use of controlled POPC/DMPS mixtures can be a valid alternative to commercial lecithin to obtain nanovectors with specific release properties.

Acknowledgements

The authors thank Prof. L. Cantú for the helpful discussion on the choice of the lipid mixture investigated. The authors also thank Mr Barbieri and Mr E. Marcotti for their help in sample preparation. This research project has been supported by the European Commission under the 6th Framework Programme through the Key Action: Strengthening the European Research Area, Research Infrastructures. Contract no. RII3-CT-2003-505925 (NMI3). This work is also based on experiments performed at the Swiss spallation neutron source SINQ, Paul Scherrer Institute, Villigen, Switzerland.

References

1 G. Barratt, *Pharm. Sci. Technol. Today*, 2000, **3**, 163–171.
2 R. Freitas, *DM, Dis.-Mon.*, 2005, **51**, 325–341.
3 M. E. Davis, Z. G. Chen and D. M. Shin, *Nat. Rev. Drug Discovery*, 2008, **7**, 771–782.
4 K. Cho, X. Wang, S. Nie, Z. G. Chen and D. M. Shin, *Clin. Cancer Res.*, 2008, **14**, 1310–1316.
5 C. Porter, K. Wasan and P. Constantinides, *Adv. Drug Delivery Rev.*, 2008, **60**, 615–616.
6 J. Oh, R. Drumright, D. Siegwart and K. Matyjaszewski, *Prog. Polym. Sci.*, 2008, **33**, 448–477.
7 S. Heuschkel, A. Goebel and R. Neubert, *J. Pharm. Sci.*, 2008, **97**, 603–631.
8 L. Zhang, F. Gu, J. Chan, A. Wang, R. Langer and O. Farokhzad, *J. Clin. Pharm. Ther.*, 2007, **83**, 761–769.
9 G. A. Hughes, *Nanomed.: Nanotechnol., Biol. Med.*, 2005, **1**, 22–30.
10 V. P. Torchilin, *Nat. Rev. Drug Discovery*, 2005, **4**, 145–160.
11 W. C. Zamboni, *Clin. Cancer Res.*, 2005, **11**, 8230–8234.
12 M. C. Pedroso de Lima, S. Simões, P. Pires, H. Faneca and N. Düzgünes, *Adv. Drug Delivery Rev.*, 2001, **47**, 277–294.
13 J. O. Rädler, I. Koltover, T. Salditt and C. R. Safinya, *Science*, 1997, **275**, 810–814.
14 F. Sonvico, A. Cagnani, A. Rossi, S. Motta, M. T. DiBari, F. Cavatorta, M. J. Alonso, A. Deriu and P. Colombo, *Int. J. Pharm.*, 2006, **324**, 67–73.
15 D. S. Kohane, N. Plesnila, S. S. Thomas, D. Le, R. Langer and M. A. Moskowitz, *Brain Res.*, 2002, **946**, 206–213.
16 S. A. Wissing, O. Kayser and R. H. Müller, *Adv. Drug Delivery Rev.*, 2004, **56**, 1257–1272.
17 J. Cao, J. Sun, X. Wang, X. Li and Y. Deng, *Drug Dev. Ind. Pharm.*, 2009, **35**, 1339–1347.
18 A. V. Boddy, E. R. Plummer, R. Todd, J. Sludden, M. Griffin, L. Robson, J. Cassidy, D. Bissett, A. Bernareggi, M. W. Verrill and A. H. Calvert, *Clin. Cancer Res.*, 2005, **11**, 7834–7840.
19 A. Rösler, G. W. Vandermeulen and H. A. Klok, *Adv. Drug Delivery Rev.*, 2001, **53**, 95–108.
20 Y. Gerelli, S. Barbieri, M. T. DiBari, A. Deriu, L. Cantù, P. Brocca, F. Sonvico, P. Colombo, R. May and S. Motta, *Langmuir*, 2008, **24**, 11378–11384.
21 V. Mourya and N. Inamdar, *J. Mater. Sci.: Mater. Med.*, 2009, **20**, 1057–1079.
22 P. Kauper and C. Laue, *U.S. Patent*, 20 090 117 195, 2009.
23 J. Suh and H. Matthew, *Biomaterials*, 2000, **21**, 2589–2598.
24 U. Keiderling, *Appl. Phys. A: Mater. Sci. Process.*, 2002, **74**, s1455–1457.
25 I. S. Gradshteyn, I. Ryzhik and A. Jeffrey, *Table of Integrals, Series, and Products*, Academic press, New York, 2007.
26 N. Kučerka, J. F. Nagle, J. N. Sachs, S. E. Feller, J. Pencer, A. Jackson and J. Katsaras, *Biophys. J.*, 2008, **95**, 2356–2367.
27 H. Schmiedel, L. Almásy and G. Klose, *Eur. Biophys. J.*, 2006, **35**, 181–189.
28 J. F. Nagle and S. Tristram-Nagle, *Biochim. Biophys. Acta*, 2000, **1469**, 159–195.
29 M. A. Kiselev, S. Wartewig, M. Janich, P. Lesieur, A. M. Kiselev, M. Ollivon and R. Neubert, *Chem. Phys. Lipids*, 2003, **123**, 31–44.
30 N. Kučerka, M. A. Kiselev and P. Balgavý, *Eur. Biophys. J.*, 2004, **33**, 328–334.
31 N. Kučerka, J. F. Nagle, S. E. Feller and P. Balgavý, *Phys. Rev. E: Stat., Nonlinear, Soft Matter Phys.*, 2004, **69**, 051903.
32 S. U. Egelhaaf, E. Wehrli, M. Muller, M. Adrian and P. Schurtenberger, *J. Microsc.*, 1996, **184**, 214–228.
33 A. Y. Grosberg, T. T. Nguyen and B. I. Shklovskii, *Rev. Mod. Phys.*, 2002, **74**, 329–345.
34 S. Zuzzi, C. Cametti, G. Onori and S. Sennato, *Phys. Rev. E: Stat., Nonlinear, Soft Matter Phys.*, 2007, **76**, 011925.
35 A. Sybachin, A. Efimova, E. Litmanovich, F. Menger and A. Yaroslavov, *Langmuir*, 2007, **23**, 10034–10039.
36 S. Sennato, F. Bordi, C. Cametti, C. Marianecci, M. Carafa and M. Cametti, *J. Phys. Chem. B*, 2008, **112**, 3720–3727.
37 F. Bordi, S. Sennato and D. Truzzolillo, *J. Phys.: Condens. Matter*, 2009, **21**, 203102.
38 G. Pabst, M. Rappolt, H. Amenitsch and P. Laggner, *Phys. Rev. E: Stat. Phys., Plasmas, Fluids, Relat. Interdiscip. Top.*, 2000, **62**, 4000–4009.
39 H. Schmiedel, P. Jorchel, M. Kiselev and G. Klose, *J. Phys. Chem. B*, 2001, **105**, 111–117.

